



CHORUS

This is the accepted manuscript made available via CHORUS. The article has been published as:

Effect of Bloch wave electron propagation and momentum-resolved signal detection on the quantitative and site-specific electron magnetic chiral dichroism of magnetic spinel oxide thin films

B. Loukya, D. S. Negi, K. Dileep, N. Pachauri, A. Gupta, and R. Datta

Phys. Rev. B **91**, 134412 — Published 10 April 2015

DOI: [10.1103/PhysRevB.91.134412](https://doi.org/10.1103/PhysRevB.91.134412)

Effect of Bloch wave electron propagation and momentum resolved signal detection on the quantitative and site-specific EMCD of magnetic spinel oxide thin films

B. Loukya,^{1,2} D. S. Negi,^{1,2} K. Dileep,^{1,2} N. Pachauri,³ A. Gupta,³ and R. Datta^{1,2,*}

¹*International Centre for Materials Science, ²Chemistry and Physics of Materials Unit, Jawaharlal Nehru Centre for Advanced Scientific Research, Bangalore 560064, India.*

³*Center for Materials for Information Technology, University of Alabama, Tuscaloosa, Alabama 35487, USA.*

Electron magnetic chiral dichroism (EMCD) in a transmission electron microscope is an element-specific magnetic characterization technique and is extremely powerful for understanding magnetism of materials at the nanoscale. However, quantitative EMCD remains a challenge. In the present report, we have highlighted and overcome major difficulties associated with the technique. For example, the experimentally observed low dichroic signal and imbalance between the L_3 and L_2 edge have been explained based on the oscillatory nature of electron propagation through the crystal thickness and specific momentum resolved signal detection, respectively. With this advancement in understanding, for the first time site-specific quantitative EMCD has been accomplished in epitaxial thin films of two important ferrimagnetic spinel oxides, NiFe_2O_4 (NFO) and CoFe_2O_4 (CFO), with varying degree of cation mixing and A site cation defects. A simple model based on phenomenological absorption has been developed for different site-specific signal contributions for the inverse spinel structure. The experimental moment values for NFO and CFO obtained using EMCD are in good agreement with first

principle based theoretical calculations and the results strengthen the promise of utilizing EMCD as a routine nanoscale magnetic characterization technique.

*Corresponding author E-mail: ranjan@jncasr.ac.in, Tel: +91 (80) 2208 2571.

I. INTRODUCTION

Electron magnetic chiral dichroism (EMCD) is element specific electron diffraction based magnetic characterization technique both for orbital (m_L) and spin (m_S) moments in a transmission electron microscope (TEM) [1-12]. EMCD is essentially equivalent to X-ray magnetic circular dichroism (XMCD) that is routinely carried out in a synchrotron, but is unique in terms of providing nanometer spatial resolution (1-2 nm) along with information obtainable from the bulk of the crystal [8,9]. Indeed, with suitable theoretical guidelines atomic-scale information can be obtained [10,11]. Though there are several reports on its development and applications to various materials, the technique is still confined to the evaluation of moment ratio (m_L/m_S) values [6,13]. This is due to the fact that the EMCD signal is dependent on a number of factors, primarily the choice of reciprocal lattice vectors, specimen thickness and K parameters, etc. [6]. Without precise determination of these parameters it is practically impossible to determine the individual m_L and m_S values for a given material using the EMCD sum rules. In the present report, we have carried out site-specific quantitative EMCD (evaluation of individual m_L and m_S values) of two different ferromagnetic spinel oxides, namely NiFe₂O₄ (NFO) and CoFe₂O₄ (CFO). As a part of this quantitative attempt, we made the following key observations.

We found that the experimental dichroic signal obtained at each L_3 and L_2 edge is much lower compared to the corresponding theoretical values and also does not vary strongly as a function of the sample thickness beyond a certain value depending on the material system and reciprocal lattice vectors. This is because of the dependence of the dichroic signal and K parameter on the sample thickness that results in the thickness averaged dichroic signal being lower than the theoretically predicted values. Additionally, it is essential to consider the thickness-averaged K parameter for any quantitative work. In this context, Wang *et. al.* [12] reported on the determination of individual moment values for NFO through the application of sum rules without explicitly mentioning the assumption of $K=3/2$ and its justification, only at which XMCD and EMCD sum rules become identical. Another important finding of our study is the observation of systematically lower dichroic signal at L_2 as compared to the L_3 edge. This is due to the method by which EMCD signal is detected. EMCD signal is detected along a particular momentum transfer direction and akin to the momentum resolved EELS technique, which yields information on the anisotropy of the electronic orbitals [14-19]. The calculation shows that this direction-dependent signal detection is responsible for the low EMCD signal at the L_2 edge compared to that at L_3 edge and the relative variation will be material and orientation-specific. This poses a serious difficulty for quantification of EMCD signal even if the thickness of the sample and the corresponding K parameter are known. Strong support from theoretical simulation is required for calculating the correction factor. In addition to this, we exploited an alternative simpler model (based on phenomenological absorption of elastic Bloch waves) to evaluate the site-specific percentage dichroic signal contributions on the total EMCD signal from the respective tetrahedral and octahedral atomic sites for a given diffraction condition. According to the experimental results, we observed consistent dichroic signal for NFO from nanoscale probing of

different regions while for CFO variation in signal is observed. This is consistent with the earlier observation of robust inverse spinel configuration for NFO and thermodynamically favored cation mixing in the case of CFO [20]. The experimentally observed moments results are supported by first principle based calculations. The results strengthen the promise of utilizing the EMCD technique as a routine quantitative characterization tool, which will be extremely valuable for unraveling novel magnetic phenomena at the nanoscale.

II. EXPERIMENTAL TECHNIQUES

Cross sectional TEM specimens were prepared by conventional mechanical polishing and Ar ion milling in order to generate large electron-transparent thin area. One plan view TEM specimen of NFO was also prepared to probe EMCD signal variation along another crystallographic axis. EMCD experiments were performed in a FEI TITAN³™ 80-300 kV aberration corrected TEM with monochromatic probe illumination. Such a probe significantly improves the signal to noise ratio during EMCD experimentation [21]. We used 2-beam geometry (2BC) since for sufficiently smaller and larger window size, i.e. $0.25G \times 0.25G$ and $0.5G \times 0.5G$ (where G represents the reciprocal vector corresponding to the EMCD experimentation, the window size will depend on the G under consideration), the difference in m_L/m_S values between 2BC and 3BC geometry are extremely small [22]. Moreover, working with 2BC geometry is found to be advantageous because of higher dichroic signal obtainable due to equal amplitude of the direct and diffracted beams. Whereas, for three beam (3BC) or systematic row of reflections case, dissimilar amplitude between direct and diffracted beams will lead to reduced EMCD signal due to the decrease in the magnitude of the imaginary part of the mixed dynamic form factor (see

section III.B for more details as well as Ref. [23]). The data processing method is described in the supplementary material and the spectra are fitted according to a fitting equation described in Ref. 24.

The X-ray magnetic circular dichroism (XMCD) spectra are simulated using WIEN2k code, [21, 25, 26] which is based on all-electron density functional theory (DFT) calculation. We have carried out XMCD calculation instead of EMCD as the latter has so far not been implemented within the WIEN2k code. There should not be any significant difference in the percentage dichroic signal between the two as the cross section expression for both are equivalent within the dipole approximation except in terms of the magnitude for the individual spectra [1,2, 23]. In addition to this, the ‘bw code’ developed for calculating percentage dichroic signal is not capable of providing spectral features necessary for the density of states (DOS)-based evaluation of the spectra [27]. Ferrimagnetic NiFe_2O_4 and CoFe_2O_4 inverse spinel structures were considered for calculating the density of states and the resultant total magnetic moment [20]. Spin-polarized and spin-orbit coupled system with orbital polarization are considered to enable the calculation of both spin and orbital moments. A dense $14 \times 14 \times 14$ k-mesh is used for integration of the Brillouin zone based on tetrahedron integration scheme. The system lattice parameters are fully relaxed by using PBE-GGA exchange correlation functional with self-consistent field cycles performed until the energy and charge values are below the convergence criterion (0.0001 Ry and 0.001 e, respectively). Force minimization is performed to obtain the forces between the atoms below 1 mRy/bohr. PBE-GGA functional cannot predict the exact excited state properties. So the recent method development by F. Tran and P. Blaha [28,29] to calculate the exact excited state properties, known as the ‘modified Becke-Johnson’ exchange correlation potential (mBJLDA),

has been used to correct the band gap in these systems,. This method is more accurate and comparatively less compute-intensive [20, 30-32]. XMCD spectra are calculated on the resultant system by calculating the matrix elements corresponding to photon absorption cross section with respect to the polarization of light and the sample magnetization within the dipole approximation [26]. The spin and orbital moments and their ratio are evaluated from the calculated spectra using the sum rules [33,34] and are compared with the DFT predicted values as given in Table 1.

III. RESULTS AND DISCUSSION

A. Discrepancy in the magnitude of dichroic signal between theory and experiment

We have consistently observed two important characteristics in the experimental EMCD spectra. Firstly, the measured dichroic signal is always smaller than the theoretical numbers obtained by first principle based calculations. Moreover, the absolute dichroic signal percentage measured by the ratio between the dichroic signals at an individual edge to the total sum signal, as what appears in the sum rules expression, is much smaller for the L_2 edge as compared to that at the L_3 edge for the investigated range of thicknesses. Figure 1 shows an example experimental EMCD spectra for NFO for $g = 400$ diffracting vector along with the theoretical XMCD spectra (see supporting information for $g = 440$). Table 1 is the summary of the obtained magnetic moments using the EMCD sum rules applied to the experimental spectra and XMCD sum rules applied to the calculated XMCD spectra and moments obtained from DFT calculations, which will frequently be referred to explain the experimental results in the subsequent text. Theoretically, we obtained essentially equal percentages of dichroic signal at L_3 and L_2 edges in the case of NFO, the maximum limit of which depends on the transition probabilities and available density

of unoccupied states (see Ref. [23] for the data on bcc-Fe, which was tested extensively for EMCD experimentation). However, the experimentally observed signal at each edge is much lower than the theoretical prediction (Fig. 1 and Table 1), and moreover the signal is lower for the L_2 edge as compared to that at the L_3 edge. The explanation for this lies in the nature of the Bloch wave electron propagation and its absorption through the crystal as well as selecting a particular momentum transfer direction during EMCD signal acquisition. While the systematic decrease in dichroic signal is not an issue (except for the signal to noise ratio) for the moment ratio evaluation, the second feature, i.e. imbalance in the signal between L_3 and L_2 edges leads to inaccurate determination of m_L/m_S ratio value unless an appropriate correction factor is incorporated. Although there is an earlier report on the percentage dichroic signal for NFO, i.e. 33% for Fe and 42% for Ni, there is no justification provided on the maximum observable limit and also these should not exceed the theoretical values [12]. Experimental dichroic spectra in Refs. 2 & 12 for Fe and NFO, respectively, also indicate a smaller dichroic signal for the L_2 edge as compared to the L_3 edge (see supporting information). We provide detailed explanation for such observations and point out the need to obtain guidance from theory for quantitative EMCD experimentation, which has not been widely utilized for magnetic characterization of materials most likely due to these practical issues not having been highlighted previously.

B. Dependence of EMCD signal on sample thickness

EMCD is an electron diffraction based technique where a pair of equally intense Bragg spots (one direct and another diffracted beam) are chosen for the simultaneous and perpendicular momentum transfer at two different positions, which are opposite to each other in the diffraction plane (Fig. 2) [2,7]. The pair of diffraction spots (0 & g) are phase shifted by $\pi/2$ and the

opposite momentum transfer, represented by $q_{\pm i}.q'$ (equivalent to two opposite helicity of incoming photons, $\sigma_{\pm i}.\sigma'$) drives the spin selected transition from $p \rightarrow d$ states ($\Delta l = \pm 1$ and $\Delta m = \pm 1$). This results in the corresponding $L_{2,3}$ absorption edges, similar to the two absorption edges resulting from the absorption of left and right circularly polarized photons in the case of XMCD. The difference between $L_{2,3}$ signal from two opposite positions on the Thales circle results in the dichroic signal. The XMCD and EMCD sum rules become mathematically equivalent, i.e. $\sigma.r \equiv q.r$ within the dipole approximation. However, the incident electron beam inside the finite crystal behaves as Bloch waves due to the periodic crystal potential and its propagation amplitude along with that of the coupled diffracted beam (within the beam representation) oscillates with sample thickness [35,36]. A small fraction of the absorption (inelastic events) of these Bloch waves by the sample volume under appropriate geometric condition (e.g., two or three beam orientation) will be responsible for the net EMCD signal. This oscillation or pendellosung phenomenon demands the proper evaluation of K parameter, which also oscillates with the sample thickness, in the EMCD sum rules in order to separately evaluate the m_L and m_S contributions.

Figure 3 shows the oscillation of direct and diffracted beam amplitudes as a function of thickness for $g = 400$ (extinction distance $\xi_g = 95.51 \text{ nm}^{-1}$, for NFO). The phenomenological absorption is taken into account (i.e., $\xi'_g = 10 \xi_g$) [35,36]. This results in variation of K parameter with the sample thickness (Fig. 3). K has been evaluated under two beam geometry according to the equation provided in Ref. 6 (see Eq. S(2) in the supporting information for the details [23], the calculation is dynamical and for two beam geometry). K varies between 0 and 3, and it is the maximum value of K where one can obtain high contrast EMCD signal at which the amplitudes of both direct and diffracted beams are equal. Therefore, it is clear that for most of the

thicknesses the amplitude of direct and diffracted beams are not the same during EMCD experiment and this results in variation in dichroic signal with sample thickness (Fig. 3) (see supporting information for the difference in variation of dichroic signal between the present case and the scenario in Ref. 37). The value of K will be different for different thicknesses and for $K = 3/2$, XMCD and EMCD sum rules become equivalent. For K greater or lower than $3/2$, there will be a concomitant increase or decrease in percentage EMCD signal as compared to the XMCD case. Moreover, it is not the single value of K for a given sample thickness; rather the thickness averaged K as well as the percentage of dichroic signal that need to be considered to explain the experimental observation of reduced signal in comparison to the theoretical prediction.

We can understand the above mentioned observation by carefully considering the oscillating nature of the Bloch wave and its absorption through the sample thickness. It is the absorption of the elastic Bloch waves that gives rise to inelastic signal (mostly comprised of phonons, plasmons and electronic excitations). A small fraction of this inelastic signal gives rise to the $L_{2,3}$ absorption edge. Only phenomenological absorption, which is a measure of the probability or counts of inelastic scattering for a given thickness with other parameters, e.g., exposure time being constant, for both the direct and diffracted beams is plotted in Fig. 4(a). This approach is similar to the treatment by Dudarev *et al* [38] but differs from the single electron Bloch wave treatment developed by Schattschneider *et al* [15]. Bloch wave model is limited in the sense that it considers only the interference term, which is only a small fraction of the inelastic waves taking part in the event and requires placing the detectors following the symmetry of the outgoing waves. While phenomenological treatment considers signals in terms of the scattering

cross section, it is also possible to trivially consider the thickness dependence of absorption. Both treatments yield essentially similar site-specific signal from spinel oxides and will be discussed further in section D. Now, to understand how the EMCD signal will vary with the sample thickness in terms of difference and its percentage with respect to the sum, let us first look at the cross section at two positions in the reciprocal space. The cross sections under two beam geometry (with incident waves as plane waves) at position 1 (+) and position 2 (-) are given by:

$$\begin{aligned}\sigma_{\pm}(E) &= \frac{\partial^2 \sigma((q \pm iq'), E)}{\partial E \partial \Omega} = C \left\{ \left| \langle \psi_f | q \cdot r | \psi_i \rangle \right|^2 + \left| \langle \psi_f | q' \cdot r | \psi_i \rangle \right|^2 \pm 2i \langle \psi_f | q' \cdot r | \psi_i \rangle \langle \psi_i | q \cdot r | \psi_f \rangle \right\} \delta(E_i - E_f + E) \\ &= C \left\{ \frac{S(\vec{q}, \vec{q}, E)}{\vec{q}^4} + \frac{S(\vec{q}', \vec{q}', E)}{\vec{q}'^4} \pm 2i \frac{S(\vec{q}, \vec{q}', E)}{\vec{q}^2 \vec{q}'^2} \right\} \delta(E_i - E_f + E) \quad \dots (1)\end{aligned}$$

Where, $C = \frac{4\gamma^2 k_f}{a_0^2 k_i}$,

γ is the relativistic factor,

a_0 Bohr radius,

k_i and k_f wave vectors before and after the interaction, respectively,

$\sigma_{\pm}(E)$ is the differential scattering cross section for two different momentum transfer directions,

$\frac{\partial^2 \sigma}{\partial E \partial \Omega}$ double differential scattering cross section,

\vec{q} and \vec{q}' are the $\pi/2$ dephased momentum transfer vectors,

r the position vector,

ψ_i and ψ_f are the initial and final state wave functions,

$\delta(E_i - E_f + E)$ is the Delta function that ensures the selected transition probability,

$S(\vec{q}, \vec{q}, E)$ and $S(\vec{q}', \vec{q}', E)$ are the dynamic form factors (DFF) for momentum transfer vectors \vec{q} and \vec{q}' , respectively,

$S(\vec{q}, \vec{q}', E)$ is the mixed dynamic form factor (MDFF).

The dichroic signal and the sum, respectively, at these two positions can be derived as

$$\nabla \sigma = \sigma_+(E) - \sigma_-(E) = 4 \frac{4\gamma^2 k_f}{a_0^2 k_i} \beta \text{Im} \left(\frac{S(\vec{q}, \vec{q}', E)}{\vec{q}^2 \vec{q}'^2} \right) \delta(E_i - E_f + E) \dots (2)$$

$$\sigma_+(E) + \sigma_-(E) = 2 \frac{4\gamma^2 k_f}{a_0^2 k_i} \left(a_1^2 \frac{S(\vec{q}, \vec{q}, E)}{\vec{q}^4} + a_2^2 \frac{S(\vec{q}', \vec{q}', E)}{\vec{q}'^4} \right) \delta(E_i - E_f + E) \dots (3)$$

where, a_1 and a_2 are the amplitudes of the direct and diffracted beams, and $\beta = 2a_1 a_2$ [5]. We consider varying amplitudes for both the direct and diffracted beam, which is in fact the practical situation. The EMCD sum rules are then written as

$$\frac{\int_{L_3} (\sigma_2 - \sigma_1) dE - 2 \int_{L_2} (\sigma_2 - \sigma_1) dE}{\int_{L_3+L_2} (\sigma_2 + \sigma_1) dE} = K \left(\frac{2 \langle S_z \rangle}{3 N_h} + \frac{7 \langle T_z \rangle}{3 N_h} \right) \dots \dots \dots (4)$$

$$\frac{\int_{L_3+L_2} (\sigma_2 - \sigma_1) dE}{\int_{L_3+L_2} (\sigma_2 + \sigma_1) dE} = K \frac{1 \langle L_z \rangle}{2 N_h} \dots \dots \dots (5)$$

where, $\sigma_1 = (\partial^2 \sigma / \partial E \partial \Omega)_{pos1}$ and $\sigma_2 = (\partial^2 \sigma / \partial E \partial \Omega)_{pos2}$. The terms $\langle S_z \rangle / N_h$, $\langle L_z \rangle / N_h$, and $\langle T_z \rangle / N_h$ are the ground-state expectation values of spin momentum, orbital momentum and magnetic-dipole operators per hole, respectively, in the d bands.

Now if K varies, then there has to be readjustment in the left hand side of Eqs. (4) & (5) accordingly, as the expectation values remains constant because these are related to the property

of the material. Figure 4(b) shows how the denominator (sum signal) and total dichroic signal (numerator) varies with thickness through the variation in a_1 and a_2 (for $g = 400$) (the calculation is dynamical and for two beam geometry). This will result in oscillation of the percentage dichroic signal with sample thickness from zero to its maximum value (Fig. 4(b)). The average dichroic signal is also shown in the same figure. For very small thickness there is a linear increase of the average dichroic signal percentage value up to 30 nm, which is $\sim 0.3 \xi_g$. The average dichroic signal is not strongly varying beyond this thickness. Experimentally, we also observe essentially the same dichroic signal with varying thicknesses. Now, for a given thickness the observed percentage dichroic signal will be given by the integrated average over the thickness, and the net resultant signal will be reduced as compared to the theoretical value. The flat dichroic signal also signifies the benefit of EMCD technique in terms of its insensitivity to sample thickness beyond a certain value as determined by the choice of reciprocal vector. The graph shown in Fig. 4(b) should be considered only as an indication of the trend in the variation of the signal with thickness but the absolute numbers can be calculated by evaluating the exact DFF (dynamic form factor) and MDFF (mixed dynamic form factor) for a given transition process. The variation of K parameter and its thickness average is shown in Fig. 4(c). The individual EMCD sum rules should therefore be modified accordingly after averaging over the sample thickness to obtain correct spin and orbital moments. However, as mentioned earlier, there is another issue regarding the imbalance in dichroic signal at individual L_3 and L_2 edges, which adds to the difficulty in extracting individual orbital and spin moments from the EMCD experiment and is discussed in detail in Section C.

C. Dependence of EMCD signal on the momentum transfer direction

Another characteristic feature we observed is that the dichroic signal percentage with respect to the total sum at L_2 edge is always lower compared to L_3 edge for both the NFO and CFO films investigated in this study. For a given thickness, approximately 3-4 times more signal in terms of percentages can be observed for L_3 edge as compared to L_2 edge (refer to Fig. 1(a) or Figs. 7 and 8). The reason behind this is related to the detection of EMCD signal along a particular momentum transfer direction with a small collection aperture. EELS is the measure of projected density of unoccupied states in the diffraction plane. Depending on the location of the detector, different types of anisotropic empty state information will be obtained. For example, it is well known from momentum resolved EELS experiments that if the detector is placed around the Bragg beams then the signal is obtained mostly along the $q \parallel z$ projected orbitals. On the other hand, if the detector is placed at some locations other than the Bragg beams, or if the sample is tilted significantly from the incoming beam direction, then the information is predominantly obtained from the perpendicular orientation governed by the $q \cdot r$ quantity. Now for a typical EMCD set up, the z and the beam direction are almost parallel, with a slight sample tilt ($\sim 4^\circ$) to achieve two-beam geometry. For $p \rightarrow d$ transitions ($L_{2,3}$ absorption edge), L_3 is mostly composed of transitions from $p_{3/2}$ to $d_{5/2} + d_{3/2}$ and L_2 is due to transitions from $p_{1/2}$ to $d_{3/2}$ states following $\Delta l = \pm 1$ and $\Delta m = 0$ selection rules corresponding to linearly polarized beam. However, for dichroic transitions the selection rule is modified to $\Delta l = \pm 1$ and $\Delta m = \pm 1$. Figure 5(a) shows the calculated orientation-averaged dichroic signal for tetrahedral Fe in NFO with partial DOS contributions included. The calculation is performed manually by selecting density of states for the specific spin-selected transitions mentioned above. Figs. 5 (b) and (c) show how the partial DOS contribution to the spectra (for tetrahedral Fe site) change in going from the orientation-averaged spectra to aperture positions $(\theta_x, \theta_y) = (0.0, 0.0)$ mrad around the direct Bragg beam and at $(\theta_x,$

$\theta_y) = (9.44, 0.0)$ mrad for one of the two typical EMCD aperture positions for $g = 440$ orientation (supporting information for the calculation details). The projected amplitude of the individual partial components on the x - y (or a - b) plane will be anisotropic and different for different orbitals. The percentage dichroic signal for each orientation is mentioned in the respective figures and one can notice the evolution of imbalance in percentage dichroic signal over L_3 and L_2 edges. We have carried out a series of calculations for other atoms in NFO (supporting information) and orientations, to show a similar imbalance between L_3 and L_2 signal in going away from direct positions (or Bragg beam) towards perpendicular q direction.

In addition to this, another point to be noted with the cubic crystal is that the appearance of diffraction pattern along three different principle crystallographic axes (i.e. x , y and z) are indistinguishable and we do not have any prior knowledge (but the crystal knows!) along which orientation the experimentation is being performed. Momentum resolved EELS experimentation will give different % dichroic signal along three different beam directions because of the anisotropy of d orbitals. The calculated results are summarized in Table 2. The experimentation along three different principle axes for NFO ($g = \langle 440 \rangle$) shows that the trend is indeed according to the theoretical prediction [23].

This has consequences on the quantitative work based on EMCD either in terms of moment ratio or their individual values. The experimental results show very high m_L/m_S ratio value due to such behavior [23]. But if one rectifies this percentage by taking theoretical guidance then the correct moment ratio values can be obtained.

D. Case study: NFO and CFO

The NFO epitaxial thin films investigated are grown on $\langle 100 \rangle$ oriented MgAl_2O_4 (MAO) substrate at 800°C temperature by a direct liquid injection chemical vapor deposition (DLI-CVD) technique developed at the University of Alabama, the details of which can be found in Ref. 39,40. The previously performed spatially resolved optical study by HREELS revealed that the films do not show any cation mixing and the stability of the inverse spinel structure is robust [20]. However, some *A* site cation vacancy regions are observed in this system [41,42]. EMCD experiments are carried out with two different diffracting vectors, 400 and 440 types and the corresponding extinction distances are ~ 95.5 and 78 nm^{-1} , respectively, which have been used in Fig. 3. These extinction distance values are calculated from average Fourier component of the crystal potential for a given periodicity and this is not an accurate description of extinction distance for spinel structure (see following discussion for the details). Intuitively, for 400 type reflection, 4B ($2\text{Fe}\uparrow+2\text{Ni}\uparrow$) planes will concentrate the channeled electrons relatively more than 2A ($2\text{Fe}\downarrow$) planes and for 440 type it is more for 4A+4B ($4\text{Fe}\downarrow+2\text{Fe}\uparrow+2\text{Ni}\uparrow$) planes as compared to 4B ($2\text{Fe}\uparrow+2\text{Ni}\uparrow$) planes. The above understanding is qualitatively developed based on relative atomic density for a given plane. Therefore, with 400 and 440 diffracting vector, signals from octahedral Fe, Ni and tetrahedral Fe were previously assumed to dominate the EMCD spectra, respectively [12]. This notion is not correct and significant contributions from other sites will be present. For $g = 400$ diffraction condition, it was previously shown that the percentage contribution from tetrahedral and octahedral Fe sites will approximately be equal i.e., 50% at the exact Bragg condition [43]. The above calculation was based on atom site dependent evaluation of EELS cross section under two beam condition (single electron model with Bloch wave

formalism) and for a given aperture position (due to the treatment of inelastic waves as Bloch waves) and specimen thickness. This calculation assumed the same average extinction distance for both the tetrahedral and octahedral 400 periodic planes, which is not the correct picture (see Fig. 6 (a) for schematic). We have taken a different and simpler approach, which provides insight into the physical processes involving electron channeling through specific atomic planes and its absorption, which is probabilistic in nature. We have calculated the Fourier component of crystal potential separately for atomic planes (e.g., 4B and 2A separately for 400 reflection) having same periodicity (400 and 440 in the present case) formed by the octahedral and tetrahedral atoms corresponding to two independent sub-lattices. Table 3 shows the atom averaged amplitude for tetrahedral and octahedral sub-lattices in NFO (similar numbers and trend are obtained for CFO). The calculation for sub-lattice contribution to the amplitude is performed in JEMS [44] after removing atoms from specific sites (e.g., to measure the effect of tetrahedral sites, the atoms from octahedral sites are removed). The average amplitude considering both the sites equals the amplitude for the lattice containing all the atoms. However, extinction distances cannot be averaged in this manner and need to be evaluated from the corresponding amplitude separately (because of reciprocal relationship). This approach gives extinction distances corresponding to $g = 400$ as 67 and 246 nm⁻¹ for octahedral and tetrahedral sub-lattices, respectively. From this, absorption per atom was evaluated for a given plane which will depend on a particular atomic density of that plane (see the supporting information for certain assumptions towards this approach). The absorption through channeling by the two sub-lattices as a function of thickness for $g = 400$ is given in Fig. 6 (b) along with percentage signal contribution from two different atomic sites. Therefore, the EMCD signal will be composed of ~51% contributions from octahedral Fe atoms and ~49% contributions from tetrahedral Fe atoms

at exact Bragg condition. For 440 reflections, the tetrahedral Fe signal will be $\sim 54\%$ (Fig. 6 (c)). The moment value evaluation carried out by Wang *et. al.* completely ignored these mixing contributions from both the sites [12]. Ignoring such contribution affects the percentage dichroic signal contribution in the sum rules and results in improper evaluation of the moment values. The confusion lies in the earlier work of authors who assumed that the tetrahedral atoms are like impurity sites and Bloch wave propagation through these can be ignored [45]. This is not true as one can clearly see the tetrahedral atoms along the zone axis imaging condition by HR-STEM, which suggests that the channeling through *A* site cations cannot be ignored relative to *B* sites [42,46]. However, if one considers all the sites then one can estimate such contributions not only at Bragg condition but as a function of deviation parameter, *s* [44]. However, the EMCD experiment with the deviation from Bragg condition is not recommended as the diffracted beam amplitude will be reduced and consequently the EMCD signal (Fig. 4 (a)). We have taken into consideration this mixing contribution from other sites along with the thickness effect on the dichroic signal and K parameter. If one corrects for such relative contributions for the values listed in Table 2 (for NFO, Fe oct, $m_s = 0.2772$, this is the value after mixing effect), then it closely matches with the DFT-based calculations. For CFO, the mixed (both *A* and *B* site contribution) spin moment values are somewhat higher (Fe oct, $m_s = 0.8563$) because of mixed cation character (see subsequent section for the discussion). The results are in very good agreement with the theory, unlike the case in Ref. 12.

We observe very low dichroic signal in most of the sample regions ($C = -1.203 \pm 0.33\%$, *C* is the % dichroic signal with respect to total sum at L_3 edge) for $g=400$ condition (Fig. 7 (a)). This is because of near cancellation of dichroic signal from the Fe residing at two different sites where

moment directions are opposite to each other. A few areas give higher values of dichroic signal (Fig. 7 (b), $C = -5.593 \pm 1.5\%$) and these correspond to *A* site cation vacancy regions (see Ref. 20, 30,39), where in the absence of *A* site cations, the net moment contributions increases from the *B* site Fe [20]. Similar observation has been made for $g = 440$ diffracting condition. For Ni the dichroic signal is relatively strong ($C = -3.13 \pm 0.58\%$) as there is no cancellation effect like as in the case of Fe (Fig. 7 (c)).

In case of CFO, the film is grown on $\langle 100 \rangle$ oriented MgAl_2O_4 (MAO) substrate at a temperature of 690°C [40]. Theoretical calculation of cohesive energy suggests that the structure can deviate from ideal inverse spinel configurations with the mixing of *B* site Co with *A* site Fe [20]. For 50% mixing case one can see that *B* site Co adopts a low spin configuration and this is compensated by *A* site Co. This means while performing experiment with 440 and 400 diffracting condition, octahedral Fe EMCD signal will dominate for 50% mixed case and for all intermediate cases $[(4-x)\text{Fe}\downarrow + x\text{Co}\downarrow + (2+x)\text{Fe}\uparrow + (2-x)\text{Co}\uparrow]$ in comparison to ideal inverse spinel configuration. For Fe, in most of the areas we observe intermediate ($C = -2.711 \pm 0.68\%$, Fig. 8 (a)) and in some areas higher ($C = -5.229 \pm 0.69\%$, Fig. 8(b)) percentage of dichroic signal from regions having mixed cases and *A* site cation defects, respectively. This is the first time that EMCD has been used to study the cation mixing effect in spinel oxide system and the uniqueness of the technique is demonstrated in comparison to its X-ray counterpart. For Co we see higher percentage of dichroic signal. This is because for mixed case, *A* site Co will have higher magnitude of moment ($2.54 \mu_B$ per atom) compared to *B* site Co ($0.81 \mu_B$ per atom) (Fig. 8(c)) [20].

IV. CONCLUSIONS

In summary, site-specific quantitative magnetic moment evaluation by EMCD is presented for two important spinel oxide thin films, NFO and CFO. Nanoscale probing of magnetism by EMCD is demonstrated to be extremely useful for obtaining spin- and orbital-specific magnetic moment information from the regular structure, as well as from the distinguishing areas with A site cation defects and mixed cation configurations for CFO. A simple model based on phenomenological absorption is presented, which is extremely useful for calculating not only the site specific contributions of signals from inverse spinel configuration but its thickness dependence as well. Regarding the EMCD technique, we have found that the dichroic signal is much lower compared to theoretically predicted values and an imbalance in the dichroic signal exists between the L_3 and L_2 edges. The former is explained by the oscillating nature of dichroic signal with sample thickness and its thickness average is less than the theoretical value. The latter observation has been related to the momentum resolved signal detection during EMCD experiment.

Acknowledgement

The authors at JNCASR sincerely acknowledge Prof. C. N. R. Rao for his constant support, funding and providing advanced transmission electron microscopy facility for this research. D. S. Negi also acknowledges CSIR, India for financial support. The work at the University of Alabama was supported by NSF ECCS Grant No.1102263.

References

- [1] C. Hébert, and P. Schattschneider, *Ultramicroscopy* **96**, 463 (2003).
- [2] P. Schattschneider, S. Rubino, C. Hébert, J. Ruzs, J. Kuneš, P. Novák, E. Carlino, M. Fabriziooli, and G. Panaccione, *Nature* **441**, 486 (2006).
- [3] J. Ruzs, P. Novák, S. Rubino, C. Hébert, and P. Schattschneider, *Acta Physica Polonica A* **113**, 599 (2008).
- [4] C. Hébert, P. Schattschneider, S. Rubino, P. Novak, J. Ruzs, and M. Stöger-Pollach, *Ultramicroscopy* **108**, 277 (2008).
- [5] B. Warot-Fonrose, F. Houdellier, M. J. Hÿtch, L. Calmels, V. Serin, and E. Snoeck, *Ultramicroscopy* **108**, 393 (2008).
- [6] L. Calmels, F. Houdellier, B. Warot-Fonrose, C. Gatel, M. J. Hÿtch, V. Serin, E. Snoeck, and P. Schattschneider, *Phys. Rev. B* **76**, 060409(R) (2007).
- [7] S. Rubino, P. Schattschneider, M. Stöger-Pollach, C. Hébert, J. Ruzs, L. Calmels, B. Warot-Fonrose, F. Houdellier, V. Serin, and P. Novak, *J. Mater. Res.* **23**, 2582 (2008).
- [8] P. Schattschneider, M. Stöger-Pollach, S. Rubino, M. Sperl, C. Hurm, J. Zweck, and J. Ruzs, *Phys. Rev. B* **78**, 104413 (2008).
- [9] P. Schattschneider, J. Verbeeck, V. Mauchamp, M. Jaouen, and A. –L. Hamon, *Phys. Rev. B* **82**, 144418 (2010).
- [10] P. Schattschneider, I. Ennen, S. Löffler, M. Stöger-Pollach, and J. Verbeeck, *J. Appl. Phys.* **107**, 09D311 (2010).
- [11] J. Ruzs, J. C. Idrobo, and S. Bhowmick, *Phys. Rev. Lett.* **113**, 145501 (2014).
- [12] Z. Q. Wang, X. Y. Zhong, R. Yu, Z. Y. Cheng, and J. Zhu, *Nat. Comm.* **4**, 1395 (2013).

- [13] J. Rusz, O. Eriksson, P. Novák, and P. M. Oppeneer, Phys. Rev. B **76**, 060408 (R) (2007).
- [14] L. Calmels, and J. Rusz, Ultramicroscopy **110**, 1042 (2010).
- [15] M. Nelhiebel, P. –H. Louf, P. Schattschneider, P. Blaha, K. Schwarz, and B. Jouffrey, Phys. Rev. B, **59**, 12807 (1999).
- [16] G. A. Botton, C. Boothroyd, and W. Stobbs, Ultramicroscopy **59**,93 (1995).
- [17] N. Nucker, H. Romberg, X. X. Xi, J. Fink, B. Gegenheimer, and Z. Zhao, Phys. Rev. B **39**, 6619 (1989).
- [18] N. D. Browning, J. Yuan, and L. M. Brown, Ultramicroscopy **38**, 291 (1991).
- [19] N. D. Browning, J. Yuan, and L. M. Brown, Phil. Mag. A **67**, 261 (1993).
- [20] K. Dileep, B. Loukya, N. Pachauri, A. Gupta, and R. Datta, J. Appl. Phys. **116**, 103505 (2014).
- [21] B. Loukya, X. Zhang, A. Gupta, and R. Datta, J. Magn. Magn. Mater. **324**, 3754 (2012).
- [22] H. Lidbaum, J. Rusz, A. Liebig, B. Hjörvarsson, P. M. Oppeneer, E. Coronel, O. Eriksson, and K. Leifer, Phys. Rev. Lett. **102**, 037201 (2009).
- [23] See Supplementary Material for the experimental EMCD spectra for $g=440$, experimental data treatment and analysis, K parameter calculation method, , calculation of percentage tetra site dichroic signal etc.
- [24] H. Lidbaum, *Transmission Electron Microscopy for Characterization of Structures, Interfaces and Magnetic Moments in Magnetic Thin Films and Multilayers*, Ph. D thesis, Uppasala University (2009).
- [25] P. Blaha, K. Schwarz, G. K. H. Madsen, D. Kvasnicka, J. Luitz, in: Proceedings of the WIEN2k, Vienna University of Technology, 2001, ISBN 3-9501031-1-2.

- [26] L. Pardini, V. Bellini, F. Manghi, and C. Ambrosch-Draxi, *Comp. Phys. Comm.* **183** (3), 628 (2012).
- [27] S. Löffler, and P. Schattschneider, *Ultramicroscopy* **110**, 831 (2010).
- [28] F. Tran, P. Blaha, *Phys. Rev. Lett.* **102**, 226401 (2009).
- [29] D. Koller, F. Tran, and P. Blaha, *Phys. Rev. B* **85**, 155109 (2012).
- [30] K. Dileep, B. Loukya, P. Silwal, A. Gupta, and R. Datta, *Journal of Physics D: Applied Physics*, **47**, 405001 (2014).
- [31] R. Sahu, K. Dileep, B. Loukya, and R. Datta, *Appl. Phys. Lett.*, **104**, 051908 (2014)
- [32] K. Dileep and R. Datta, *Journal of Alloys and Compounds*, **586**, 499 (2014)
- [33] B. T. Thole, P. Carra, F. Sette, and G. V. Laan, *Phys. Rev. Lett.* **68**, 1943 (1992).
- [34] C. T. Chen, Y. U. Idzerda, H. -J. Lin, N. V. Smith, G. Meigs, E. Chaban, G. H. Ho, E. Pellegrin, and F. Sette, *Phys. Rev. Lett.* **75**, 152 (1995).
- [35] B. Fultz, and J. M. Howe, *Transmission Electron Microscopy and Diffractometry of Materials*, 3rd edn., Heidelberg Springer, 2008.
- [36] D. B. Williams, C. B. Carter, *Transmission Electron Microscopy: A Text Book for Materials Science*, second ed., Springer, New York, 2009.
- [37] J. Ruzs, S. Rubino, and P. Schattschneider, *Phys. Rev. B* **75**, 214425 (2007).
- [38] S. L. Dudarev, L. M. Peng, and M. J. Whelan, *Phys. Rev. B* **48**, 13408 (1993).
- [39] J. X. Ma, D. Mazumdar, G. Kim, H. Sato, N. Z. Bao, and A. Gupta, *J. Appl. Phys.* **108**, 063917 (2010).
- [40] L. Shen, M. Althammer, N. Pachauri, B. Loukya, R. Datta, M. Iliev, N. Bao, and A. Gupta, *J. Cryst. Growth* **390**, 61 (2014).

- [41] R. Datta, S. Kanuri, S. V. Karthik, D. Mazumdar, J. X. Ma, and A. Gupta, *Appl. Phys. Lett.* **97**, 071907 (2010).
- [42] R. Datta, B. Loukya, N. Li, and A. Gupta, *J. Cryst. Growth* **345**, 44 (2012)
- [43] K. Tatsumi, S. Muto, and J. Rusz, *Microsc. Microanal.* **19**, 1586 (2014).
- [44] P. Stadelmann, *JEMS Electron Microscopy Software*, 1999-2009.
- [45] J. Taftø, and L. Krivanek, *Phys. Rev. Lett.* **48**, 560 (1982).
- [46] K. Tatsumi, and S. Muto, *J. Phys.: Condens. Matter* **21**, 104213 (2009).

List of Figures:

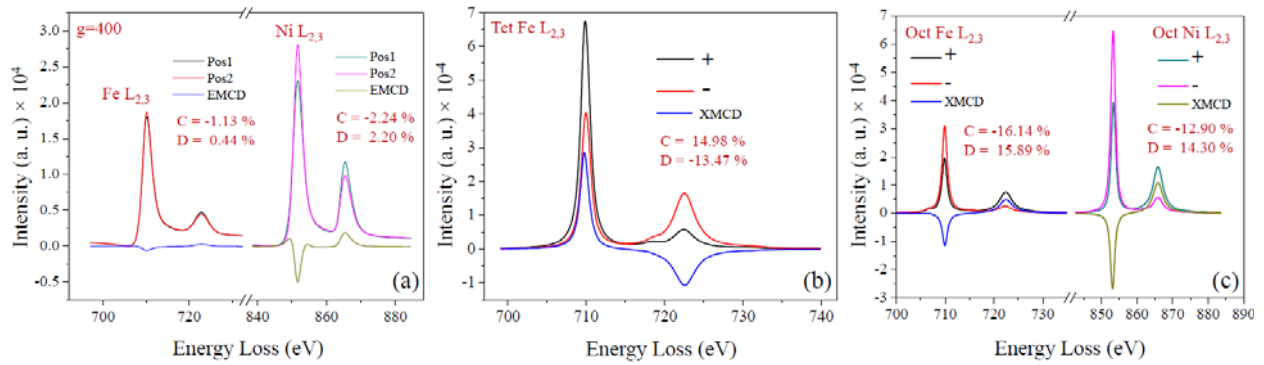


FIG.1. (Color Online) (a) Experimental example EMCD $L_{2,3}$ spectra and dichroic signal for Fe at both tetrahedral and octahedral and Ni at octahedral sites in NiFe_2O_4 . C and D are the % dichroic signal with respect to total sum at L_3 and L_2 edge, respectively. (b) and (c) Theoretical XMCD plots for atoms at the two sites. The graph shows discrepancy between experimental and theoretical EMCD percentage in terms of magnitude of signals and imbalance between L_2 and L_3 dichroic signal.

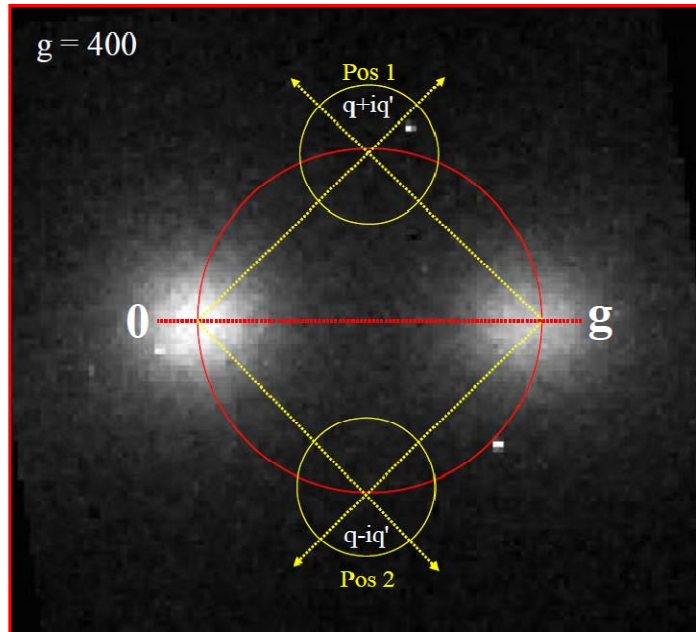


FIG. 2. (Color Online) EMCD experimental geometry showing perpendicular momentum transfer simultaneously by the direct and one of the diffracted beams (in this case $g = 400$) under two beam excitation. Simultaneous momentum transfer at two opposite positions represented by $q \pm i \cdot q'$ is equivalent to two different helicity of incoming photons as $\pm i \cdot q'$ in case of XMCD.

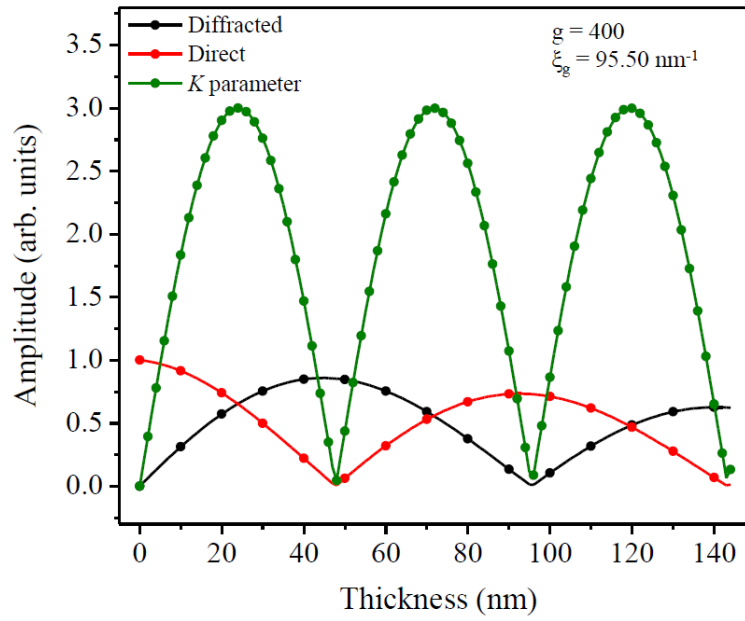


FIG. 3. (Color Online) Direct and diffracted beam oscillations as they propagate through the sample thickness for $g = 400$ of NFO. Variation of K parameter with thickness is also shown. The extinction distance is $\zeta_g = 95.51 \text{ nm}^{-1}$.

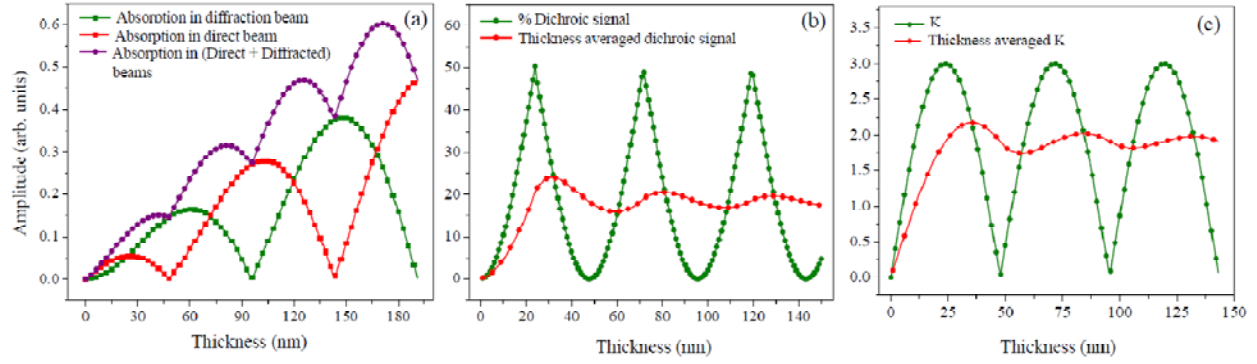


FIG. 4. (Color Online) (a) Absorption part of both direct and diffracted beams ($g = 400$) along with total absorption as a function of sample thickness for $g = 400$ of NFO under two beam orientation. Oscillation and thickness averaged (b) % dichroic signal (with respect to total sum), this has been plotted considering equal amplitude of either direct or diffracted wave whenever they occur with sample thickness and (c) K parameter with sample thickness are shown. Both % dichroic signal and K parameter become almost flat beyond a certain thickness thus favoring experimental evaluation of moment values.

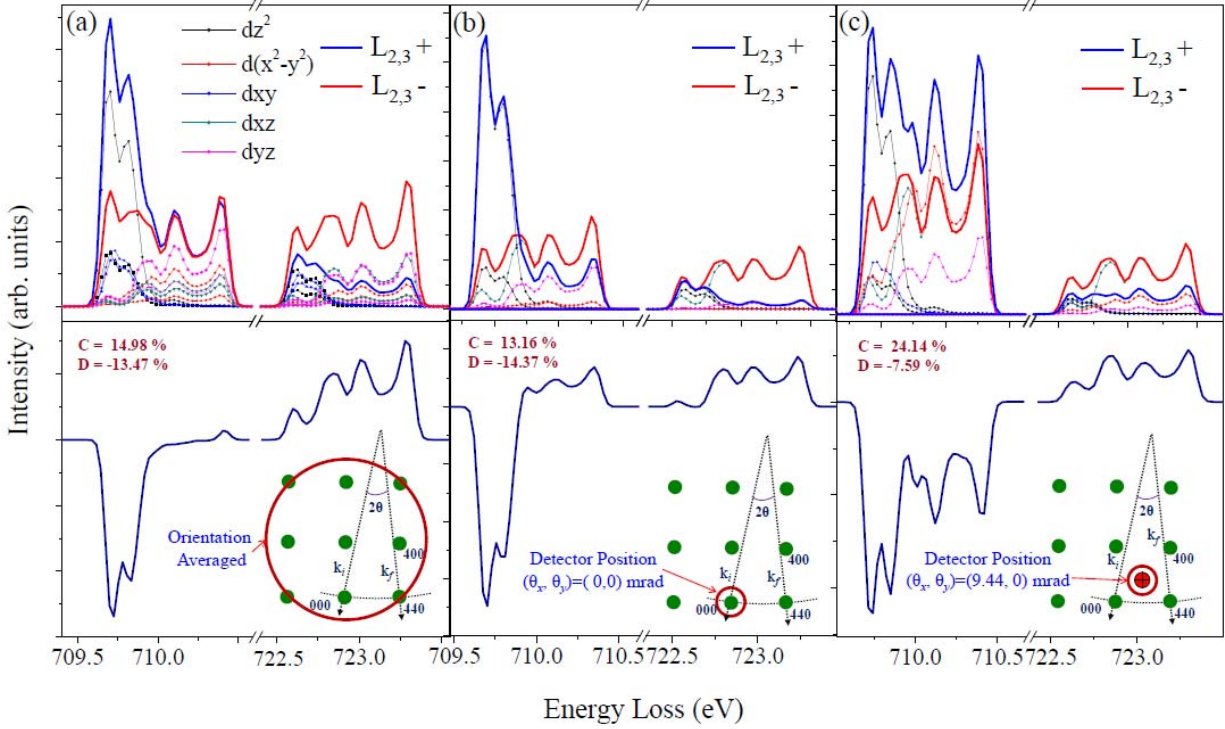


FIG. 5. (Color Online) (a) Orientation-averaged theoretical EMCD spectra along with relative orbital contributions for Fe_{tet} site in NFO with $g = 440$ diffracting condition. (b) Momentum resolved EMCD with incoming beam parallel to z axis of the crystal and detector position at $(\theta_x, \theta_y) = (0.0, 0.0)$ with 2 mrad collection aperture. (c) Momentum resolved EMCD for detector position at $(\theta_x, \theta_y) = (9.44, 0.0)$, which is typically one of the EMCD aperture positions, with same 2 mrad. collection aperture. One can observe the development of imbalance in EMCD signal between L_3 and L_2 edges. Similar observations were made for atoms at other sites, e.g., Fe_{Oct} and Ni_{Oct} and the details are given in supporting information.

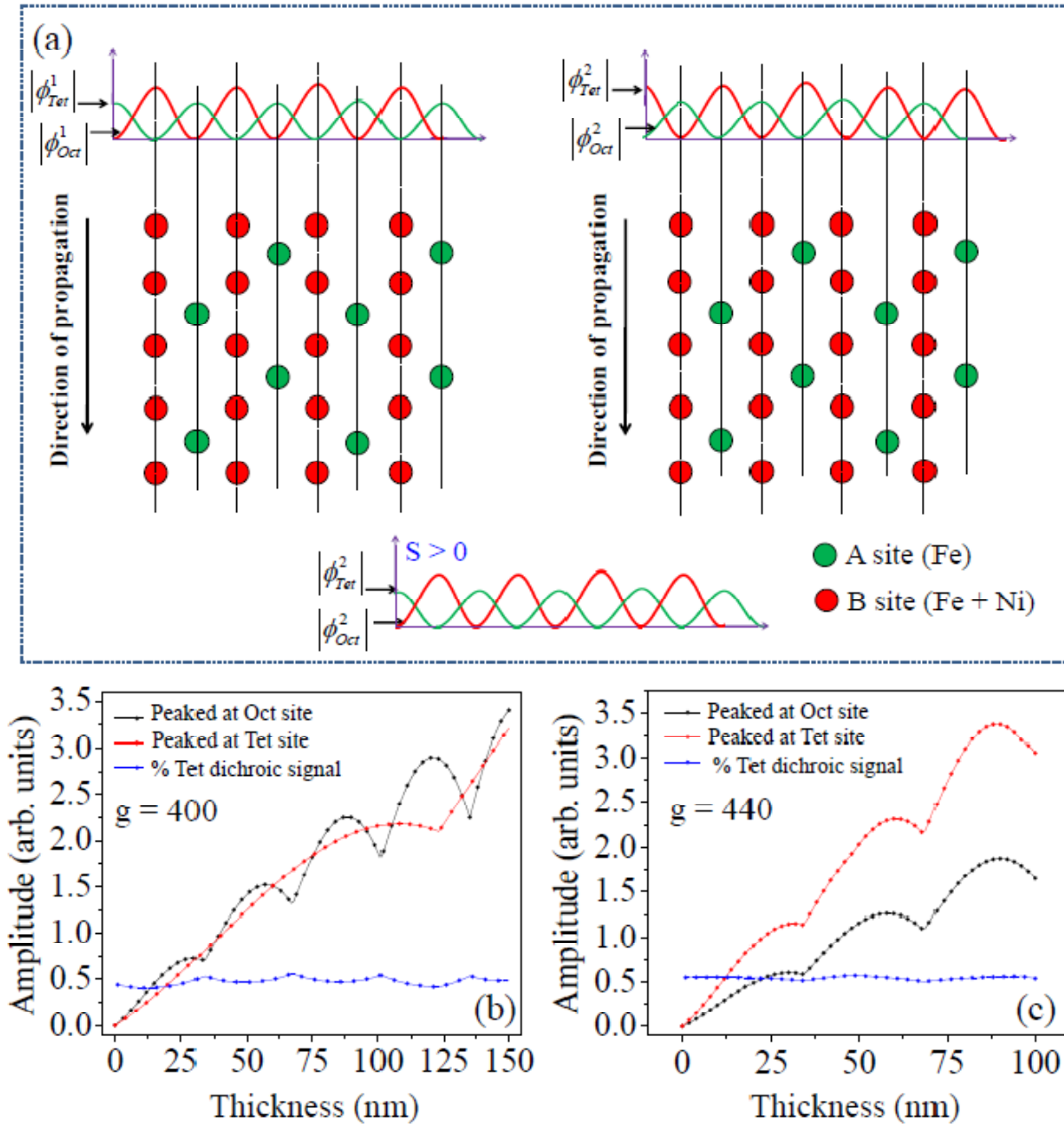


FIG. 6. (Color Online) (a) Two independent sublattice based model for inverse spinel structure where Bloch waves corresponding to tetrahedral and octahedral symmetry are shown. Percentage signal contribution from tetrahedral Fe site relative to octahedral site with (b) $g = 400$ and (c) with $g = 440$ diffracting condition. The % contribution does not oscillate strongly with thickness and shows almost constant value.

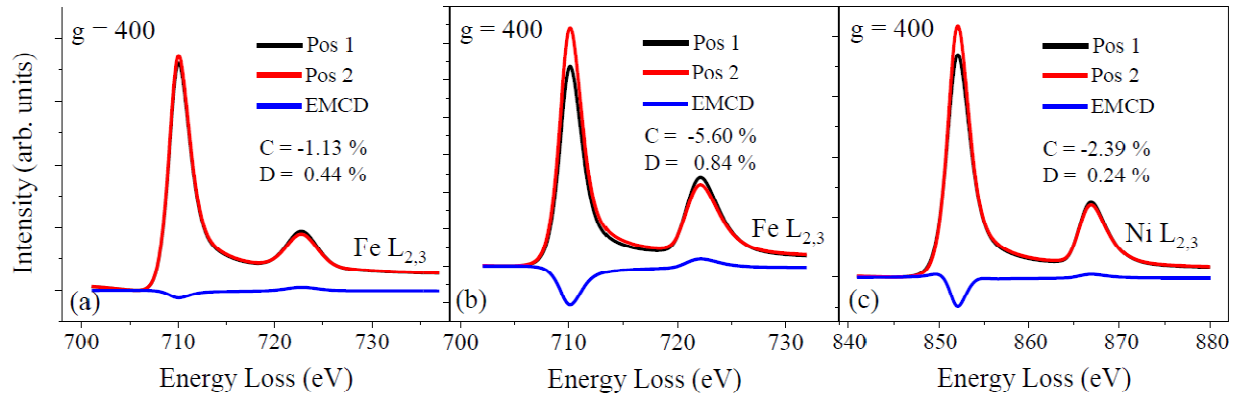


FIG. 7. (Color Online) Example EMCD spectra for NFO with $g = 400$ diffracting vector. (a) From ideal inverse spinel structure and (b) from A site cation defect area from Fe. (c) EMCD spectra from Ni. For $g = 440$ see supporting information.

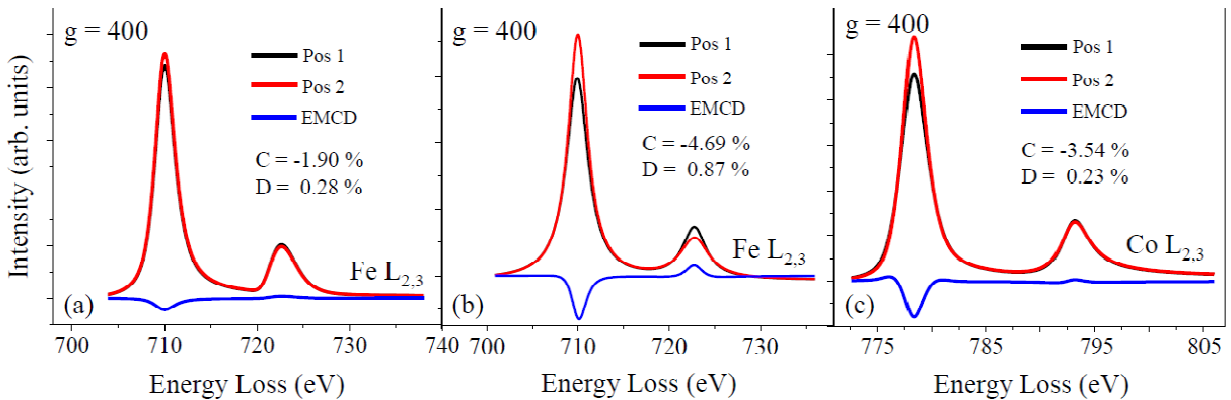


FIG. 8. (Color Online) (a) Example EMCD spectra for CFO with $g = 400$ diffracting vector. (a) EMCD signal from ideal inverse spinel area and (b) from cation mixed area from Fe. (c) EMCD spectra from Co. For $g = 440$ see supporting information.

List of Tables:

TABLE 1: Orbital (m_l) and spin (m_s) specific moment values for NFO obtained from the experimental results on NFO and CFO and by applying XMCD sum rules on the calculated XMCD spectra and from the density functional theory based (Wien2k) calculations, for the ideal inverse spinel configuration. The experimental moment values for Oct Fe is not corrected for signal mixing from A site Fe but corrected for the imbalance due to particular momentum selection direction.

Structure	EMCD sum rules on expt. Spectra (μ_B/atom)		XMCD sum rules on cal. spectra m_L/m_S	From Wien2k calculation (μ_B/atom)		
	m_L	m_S		m_L	m_S	m_L/m_S
Tet Fe	--	--	0.024	0.0075	4.1142	0.0018
NFO Oct Ni	--	--	-0.0223	-0.0500	-1.8031	0.0277
Oct Fe	-0.0061	-0.2772	-0.0034	-0.0070	-4.2076	0.0016
Tet Fe	--	--	0.0238	0.0076	4.1290	0.0018
CFO Oct Co	--	--	0.0130	-0.0408	-3.6727	0.0111
Oct Fe	-0.0190	-0.8563	0.0194	-0.0081	-4.1928	0.00193

TABLE 2: Variations in dichroic percentages along three different principle axes with two different detector positions.

	X - Orientation				Y - Orientation				Z - Orientation			
	$(\theta_x, \theta_y)=(0,0)$		$(\theta_x, \theta_y)=(9.44,0)$		$(\theta_x, \theta_y)=(0,0)$		$(\theta_x, \theta_y)=(9.44,0)$		$(\theta_x, \theta_y)=(0, 0)$		$(\theta_x, \theta_y)=(9.44,0)$	
NFO	L ₃	L ₂	L ₃	L ₂	L ₃	L ₂	L ₃	L ₂	L ₃	L ₂	L ₃	L ₂
Tet Fe	-26.37	5.09	-26.31	3.57	-21.16	10.33	-14.49	10.44	-13.16	14.37	-24.14	7.59

TABLE 3: Tetrahedral and octahedral sub lattice dependent amplitude and extinction distances for NFO and CFO structures.

Structure	Diffracting plane	Tetrahedral Lattice		Octahedral Lattice	
		Ext. Dist. (nm ⁻¹)	Amplitude (Vol ⁻¹)	Ext. Dist. (nm ⁻¹)	Amplitude (Vol ⁻¹)
NFO	(400)	375.24	2.04	67.45	11.32
	(440)	132.41	5.77	96.14	7.96
CFO	(400)	422.02	1.81	67.37	11.34
	(440)	139.69	5.46	96.12	7.94